Article

Investigation on Condensation Characteristics and Removal Performance of SO₃ in Low-Low-Temperature Electrostatic Precipitator

Zongkang Sun [1,2], Heng Chen [2,*] and Linjun Yang [2,*]

[1] Guangdong Electric Power Development Co., Ltd., Guangzhou 510030, China; sunzongkang@geg.com.cn
[2] Key Laboratory of Energy Thermal Conversion and Control of Ministry of Education, School of Energy and Environment, Southeast University, Nanjing 210096, China
* Correspondence: 230208526@seu.edu.cn (H.C.); ylj@seu.edu.cn (L.Y.)

Abstract: The low-low-temperature electrostatic precipitator (LLT-ESP) is considered one of the mainstream technological approaches for achieving ultra-low ash emissions and has already been applied in many coal-fired power plants. Particulate matter and SO₃ can both be removed by LLT-ESP. However, the removal performance of SO₃ is relatively lower than that of particulate matter, which is caused by the condensation characteristics of SO₃. In this paper, the condensation characteristics of SO₃ were investigated on a simulated experimental system, and several measurement and characteristic methods were used to investigate mechanisms. After reducing the flue gas temperature with a heat exchanger, the size distribution of particulate matter, the mass concentration of SO₃ on different sizes of particulate matter, as well as the microscopic morphology and elemental composition of particulate matter, were all experimentally studied. The results indicate that gaseous SO₃ transformed into a liquid phase by heterogeneous or homogeneous condensation and then adhered to the surface of particulate matter through nucleation–condensation, collision–coalescence, and adsorption reactions. Furthermore, the removal efficiency of SO₃ in LLT-ESP was also investigated under various conditions, such as ash concentration and flue gas temperature drop, suggesting that a higher ash concentration and a more significant temperature drop were beneficial for improving SO₃ removal efficiency. Nevertheless, it is worth noting that the impact was limited by a further increase in ash concentration and a drop in flue gas temperature.

Keywords: SO₃; condensation; removal; LLT-ESP; coal-fired flue gas

1. Introduction

In recent years, due to the comprehensive implementation of ultra-low emission standards for coal-fired power plants in China, the retrofitting of low-low-temperature electrostatic precipitators (LLT-ESPs) has become one of the mainstream technological approaches for achieving ultra-low ash emissions [1–3]. The "LLT-ESP" is a device that includes a heat exchanger in front of the traditional electrostatic precipitator (ESP) [4], leading to a reduction in flue gas temperature from approximately 120–160 °C to below the acid dew point, typically around 90 °C [5,6]. For SO₃ in flue gas, its existence form changes as the flue gas temperature decreases [7]. When the flue gas temperature is above 400 °C, SO₃ primarily exists in its gaseous form as SO₃ [8,9]. As the flue gas temperature drops below 205 °C, almost all of the SO₃ combines with the vapor in the flue gas [10,11], transforming into gaseous H₂SO₄ [12]. As the flue gas temperature continues to decrease below the acid dew point [13], gaseous H₂SO₄ begins to condense, forming sulfuric acid droplets [14]. The existence form of SO₃ with flue gas temperature variation is fully utilized in LLT-ESP, where the flue gas temperature drops below the acid dew point, and the gaseous SO₃ transitions into liquid H₂SO₄ by heterogeneous or homogeneous condensation [15,16]. In the case of heterogeneous condensation, sulfuric acid droplets

adhere to the surface of particulate matter, leading to a substantial reduction in its electrical resistance [17], which is beneficial for promoting ash removal performance in ESPs [18,19]. In the case of homogeneous condensation, the substantial formation of sulfuric acid droplets promotes the adhesion and coalescence of particulate matter, resulting in the enlargement of particulate matter, which also improves the ash removal efficiency of ESPs [20].

The synergistic removal effect of SO_3 and particulate matter in LLT-ESPs has already been confirmed [21]. It has been reported that there is significant gas-to-particle conversion of SO_3 in the heat exchanger before ESP, with approximately 30–90% of gaseous SO_3 undergoing this transition [22]. In ESPs, most condensed SO_3 and particulate matter are effectively removed. Typically, the removal efficiency of SO_3 in LLT-ESPs ranges from 60% to 90%, closely related to the condensation characteristics of gaseous SO_3 [22]. Nevertheless, the removal efficiency of SO_3 in LLT-ESPs in different coal-fired power plants is significantly different [23]. In the process of LLT-ESP, the sulfuric acid droplets formed below the acid dew point temperature are of relatively small sizes [24], and some sulfuric acid droplets may not effectively adsorb or combine with particulate matter before entering the ESP [25], leading to a low removal efficiency of SO_3 compared to particulate matter [26]. That is, when the flue gas contains a high SO_3 concentration, more SO_3 may condense by homogeneous condensation, and thus the generated sulfuric acid droplets are in the submicron size range, which is difficult to remove effectively [27].

Many efforts have been made to evaluate the condensation characteristics of SO_3 in LLT-ESPs [28], and a qualitative description is given by experimental investigations based on coal-fired flue gas [29]. However, due to the inevitable presence of SO_3 in coal-fired flue gas, the condensation characteristics of SO_3 were investigated in the presence of both SO_3 and fly ash [30], which makes it challenging to investigate the impact of fly ash, especially particulate matter, on the condensation characteristics of SO_3. The precise understanding of the condensation characteristics of SO_3 is of great significance for improving the synergistic removal efficiency of both SO_3 and fly ash, assessing the corrosion risk of heat exchangers in LLT-ESPs, and optimizing the operational parameters of LLT-ESPs.

A simulated experimental system was established in this work, and some distinctive measurement and sampling methods were also proposed to investigate SO_3 condensation characteristics. Given that the fly ash was the necessary component, the SO_3 condensation characteristics were investigated in the conditions of with or without ash. The size distribution and microscopic morphology of particles before and after the flue gas temperature drop were investigated, as well as the mass concentration of SO_3 on different sizes of particulate matter. Additionally, the mineral composition was determined by XRD, and the SO_3 condensation characteristics were determined by sulfur (S) element content using EDS analysis. Furthermore, the influence of ash concentration and flue gas temperature drop on the removal efficiency of SO_3 in an LLT-ESP was also studied. The results could further reveal the SO_3 condensation characteristics in LLT-ESPs and the key influencing factors for SO_3 removal performance, which would provide the theoretical foundation and engineering guidance for the design and operation of LLT-ESPs.

2. Experimental Section

2.1. Experimental Apparatus

The experimental system mainly consisted of a forced draft fan, a gas heater, a buffer vessel, a heat exchanger, an ESP, and an induced draft fan, as shown in Figure 1. With the combined action of the forced draft fan and gas heater, approximately 300 Nm^3/h of air could be heated to 150 °C. In the buffer vessel, a steam generator, SO_3 generator, and solid aerosol generator were employed to adjust the vapor concentration, SO_3 concentration, and ash concentration in hot gas, respectively. In the heat exchanger, the simulated hot flue gas containing vapor, SO_3, and ash was cooled to an appropriate temperature, and the sampling points were set at the inlet and outlet of the heat exchanger. The ESP used to remove particles in flue gas was a barb-plate-type ESP with an operating voltage of −40 kV.

The purified simulated flue gas was discharged into the atmosphere through the induced draft fan, and an SO_3 sampling point was set at the inlet of the induced draft fan.
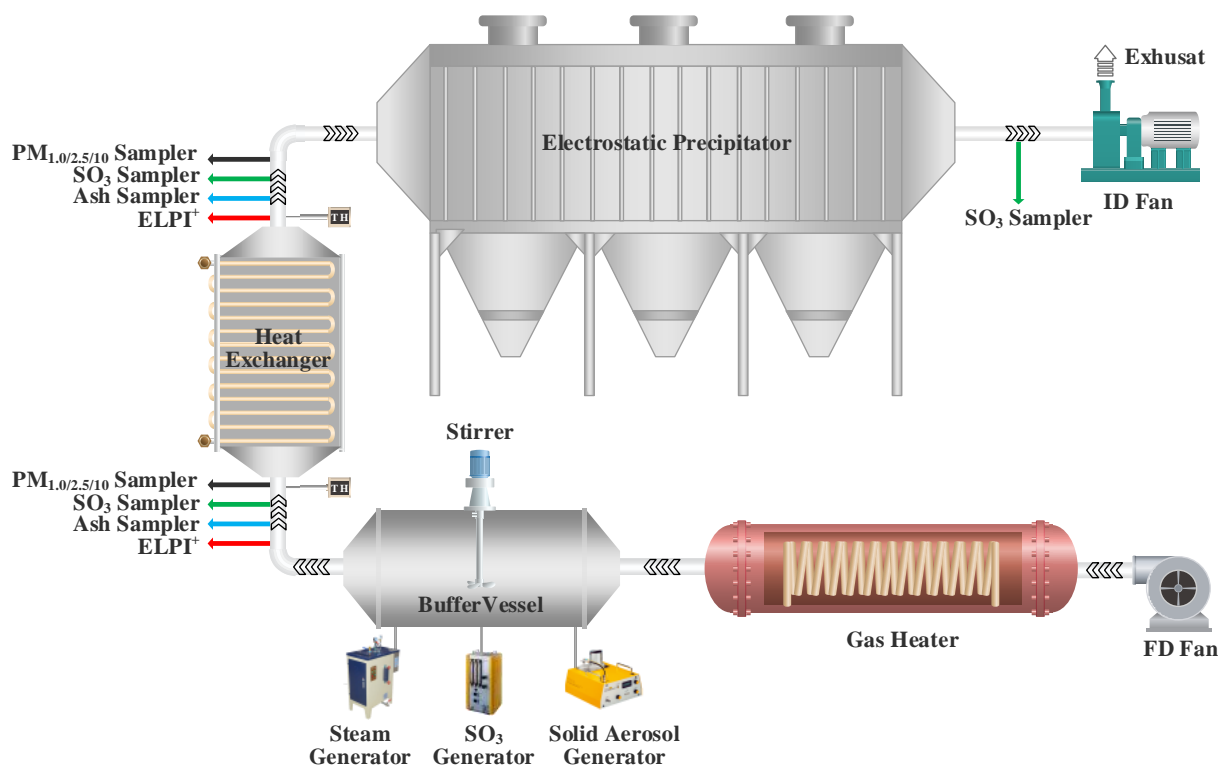

Figure 1. Schematic diagram of experimental system.

2.2. Measurement Method

In our experiments, the sampling of SO_3 was conducted using an improved method based on China's national environmental protection standard (HJ 544-2016), as illustrated in Figure 2 [31]. Flue gas containing SO_3 and ash was entered into a $PM_{1.0/2.5/10}$ impactor with an external heating jacket (PMS-410, Dekati Co., Ltd., Tampere, Finland) through an isokinetic sampling nozzle and a heated sampling probe. The heating temperature of the sampling probe and heating jacket was set to the same temperature as the sampling point. The particulate matter, including ash and condensed sulfuric acid droplets, in the flue gas could be captured by the impact plates and filters inside the $PM_{1.0/2.5/10}$ impactor. The gaseous SO_3 passed through two absorption bottles, where gaseous SO_3 would be absorbed by the absorption solution. By measuring the concentration of SO_4^{2-} in the absorption solution and combining it with the sampling flue gas volume, the concentration of gaseous SO_3 in the flue gas could be calculated.
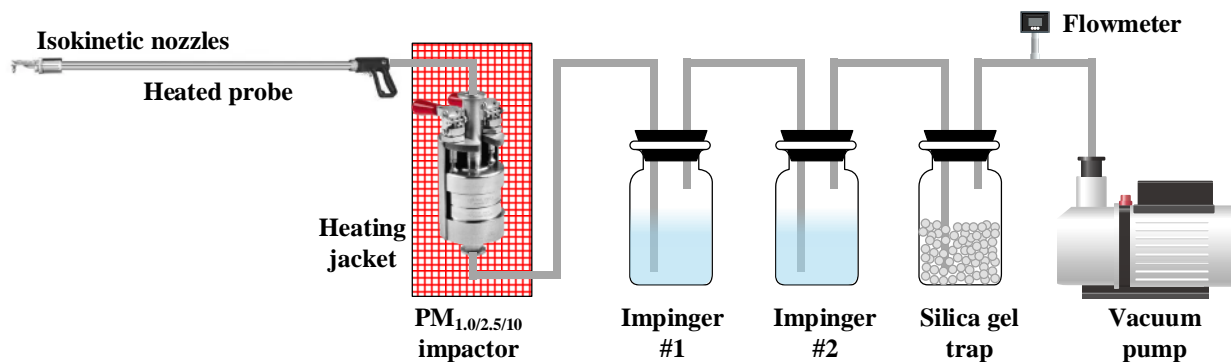

Figure 2. SO_3 sampling system.

The size distributions and concentrations of particles (including ash and condensed sulfuric acid droplets) were measured by an electrical low-pressure impactor (ELPI$^+$, Dekati Co., Ltd., Tampere, Finland), which consists of 15 stages, and the measurement range was from 0.006 to 10 μm. The moisture of the flue gas was determined by a flue gas moisture analyzer (HMS545P, Janapo, Nanjing, China), and the ash concentration was obtained by an aspirated isokinetic sampler (WJ-60B, Laoying Ltd., Qingdao, China). The particles' microscopic morphology was observed using field emission scanning electron microscopy (Ultra Plus, Zeiss Ltd., Oberkochen, Germany) with an acceleration voltage of 2 kV. The S element content in the ash was analyzed using an energy-dispersive spectrometer (X-MAX, Oxford, UK). X-ray diffraction (XRD) was employed to determine the mineral composition, with a scanning range of 2θ = 5–90°.

2.3. Calculation

In this work, the mass concentration of SO$_3$ in ash with different particle sizes was defined as follows:

$$M_{SO_3} = \frac{m_{SO_3}}{m_{ash}} \tag{1}$$

where M_{SO_3} was the SO$_3$ mass concentration in ash at a certain stage of ELPI$^+$ or the PM$_{1.0/2.5/10}$ impactor (μg/mg), m_{SO_3} was the SO$_3$ mass in ash at this stage (μg), and m_{ash} was the ash mass at this stage (mg).

In addition, the SO$_3$ removal efficiency was defined as follows:

$$\eta_{SO_3} = \frac{m_{in} - m_{out}}{m_{in}} \times 100\% \tag{2}$$

where η_{SO_3} was the SO$_3$ removal efficiency (%), m_{in} was the SO$_3$ concentration before LTT-ESP (mg/Nm^3), and m_{out} was the SO$_3$ concentration after LTT-ESP (mg/Nm^3). It is worth noting that the SO$_3$ concentration in flue gas is an aggregated concentration of both gaseous SO$_3$ concentration and condensed SO$_3$ concentration

3. Results and Discussion

3.1. The Condensation Characteristics of SO$_3$ in LLT-ESP

3.1.1. Size Distribution of Particles after Heat Exchanger

In order to investigate the condensation characteristics of SO$_3$ on ash, ELPI$^+$ was used to measure the particle size distribution of particles in the flue gas after the heat exchanger in cases where only SO$_3$ was present, only ash was present, and both were present. In experiments, the flue gas temperatures before and after the heat exchanger were about 150 °C and 90 °C, similar to the actual situation in a coal-fired plant.

It can be seen from Figure 3 that when only SO$_3$ was present, a large number of sulfuric acid droplets were generated after the heat exchanger. The size distribution of sulfuric acid droplets exhibited a unimodal distribution with a peak at 0.02 μm, and the majority of sulfuric acid droplet sizes were smaller than 0.1 μm, accounting for 95.2% of the total. In the case where only fly ash was present, it was noted that the size distribution of ash exhibited a bimodal distribution with peaks at 0.04 and 1.25 μm. In contrast, when both SO$_3$ and fly ash coexisted in the flue gas, it was found that the particulate matter size distribution also exhibited a bimodal distribution, with peak particulate matter sizes of 0.02 μm and 1.25 μm. Additionally, it was noted that the concentration of particulate matter below 0.11 μm was lower in this case compared to when only SO$_3$ was present, indicating that the presence of fly ash in flue gas leads to a reduction in the concentration of sulfuric acid liquid droplets. When the flue gas passed through the heat exchanger and the temperature decreased, some gaseous H$_2$SO$_4$ in the flue gas underwent homogeneous condensation, forming sulfuric acid droplets with smaller particle sizes and larger quantities [32,33]. When only SO$_3$ was present in the flue gas, the lack of condensation nuclei required for heterogeneous condensation resulted in predominantly homogeneous condensation of gaseous SO$_3$. The role of nucleation sites is to provide a site for the attachment and growth of liquid sulfuric

acid droplets during the condensation process of gaseous SO_3 [34,35]. As a result, a large number of small sulfuric acid liquid droplets are formed. However, when both fly ash and SO_3 were present in the flue gas, both heterogeneous and homogeneous condensation of gaseous SO_3 occurred simultaneously. Some gaseous SO_3 condenses into droplets with fly ash acting as condensation nuclei, and adherence to these particles occurs. Another portion of gaseous SO_3 undergoes homogeneous condensation to form sulfuric acid droplets. These droplets further adhere to fly ash through collision, reducing the concentration of residual sulfuric acid droplets in the flue gas due to the combined effects of both mechanisms.
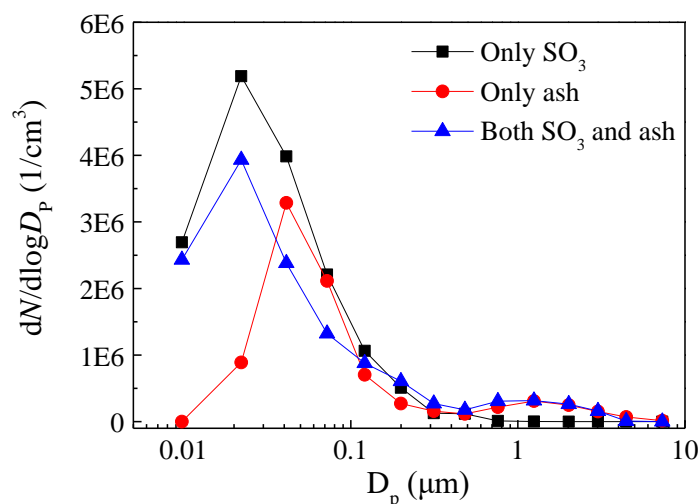

Figure 3. Size distribution of particulate matter after heat exchanger in different conditions (the flue gas temperatures before and after the heat exchanger were about 150 °C and 90 °C).

3.1.2. Mass Concentration of SO_3 on Ash with Different Sizes

It was mentioned above that when both SO_3 and fly ash were present in the flue gas, heterogeneous condensation of SO_3 occurred. Gaseous SO_3 would condense into liquid droplets, with fly ash acting as condensation nuclei. Therefore, to further investigate the condensation characteristics of SO_3, a $PM_{1.0/2.5/10}$ sampler was used to collect fly ash in the flue gas after the heat exchanger, and the mass concentration of SO_3 in four particle size ranges of the sampler was analyzed and tested.

As observed in Figure 4, after passing through the heat exchanger, the mass concentrations of SO_3 condensed on fly ash in four particle size ranges were increased. A more significant increase can be observed as the fly ash size decreases. Notably, in fine particulate matter below 1.0 μm, the increase in the mass concentration of SO_3 was most pronounced, rising from 45.6 μg/mg to 152.7 μg/mg. This indicated that SO_3 had a stronger tendency to condense on smaller particulate matter, with the majority of condensation occurring in particulate matter below 1.0 μm. Based on the above analysis, it can be concluded that during the condensation of gaseous H_2SO_4, both heterogeneous and homogeneous condensation processes occurred. In the heterogeneous condensation process, H_2SO_4 condensed on particulate matter as condensation nuclei. Smaller particulate matter with larger surface areas provided more surface area for condensation under the same mass conditions, resulting in more sulfuric acid droplets forming on smaller particulate matter under the same conditions. Additionally, in the homogeneous condensation process, gaseous H_2SO_4 condensed into extremely fine sulfuric acid droplets and adhered to particulate matter through collisions. In this case, a higher quantity of smaller particulate matter led to a greater collision probability with sulfuric acid droplets, resulting in a higher quantity of sulfuric acid droplets adhering to smaller particulate matter through collisions. Thus, it was evident that during the low-temperature electrostatic dust removal process, SO_3 was more likely to condense on smaller particulate matter.
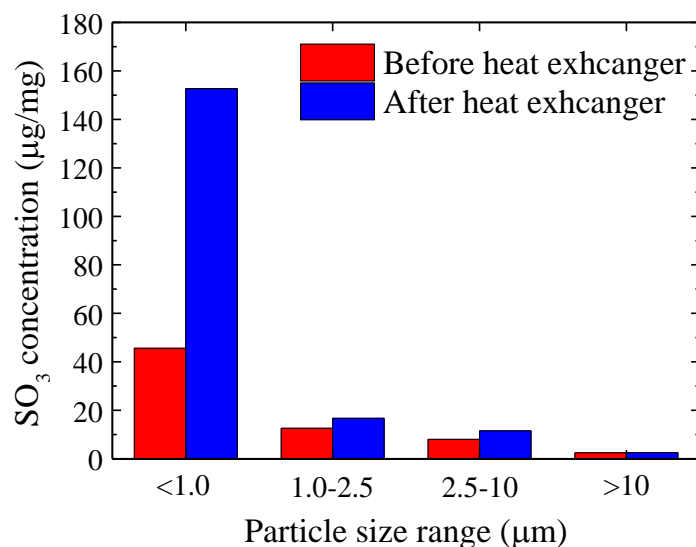
Figure 4. SO_3 concentration on ash before and after heat exchanger (sampled by $PM_{1.0/2.5/10}$ impactor).

To further investigate the condensation characteristics of SO_3 on particulate matter of different sizes, samples of particulate matter from different size ranges were collected using ELPI+ and the mass concentrations of SO_3 were tested, as shown in Figure 5. ELPI+ had 14 internal serial impactors, and the correspondence between the impactor stages and particulate matter size ranges is provided in Table 1. From Figure 4, it can be observed that the mass concentration of SO_3 in particulate matter significantly increased in stages 3 to 6, which corresponded to particulate matter size ranges from 0.03 to 0.26 µm. The total mass concentration of SO_3 in these four fine particulate matter stages increased from 31.3 µg/mg to 119.6 µg/mg. The most significant increase occurred in stage 5, where the mass concentration of SO_3 increased from 8.3 µg/mg to 56 µg/mg. It is worth noting that the mass concentration of SO_3 in fine particulate matter within the 0.1 µm range did not increase as particulate matter size decreased. The reason for this was that in stages 1 and 2, the concentration of particulate matter in the particulate matter size range was low, resulting in a lower collision probability between condensing sulfuric acid droplets and these particulate matter. Thus, a significant amount of SO_3 did not condense on fly ash in this particulate matter size range. This indicated that the condensation of SO_3 was influenced by both the particulate matter surface area and the concentration of particulate matter. In other words, SO_3 condensation was controlled by both heterogeneous and homogeneous condensation mechanisms simultaneously.
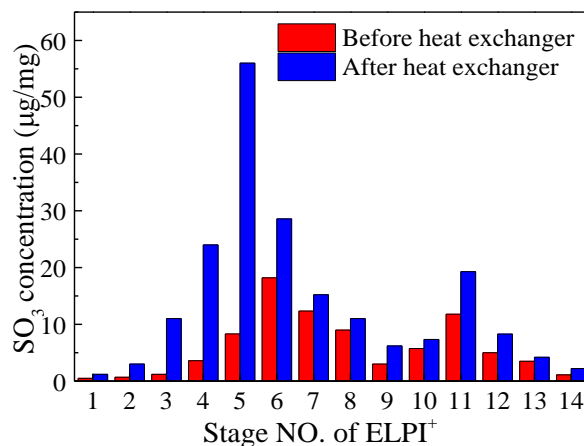

Figure 5. SO_3 concentration on ash before and after heat exchanger (sampled by ELPI+).

Table 1. Correspondence between the number of ELPI$^+$ impactor.

Stage NO. of ELPI$^+$	Size Range of Particles (µm)	Stage NO. of ELPI$^+$	Size Range of Particles (µm)
1	0.006~0.0159	8	0.384~0.605
2	0.0159~0.0308	9	0.605~0.952
3	0.0308~0.055	10	0.952~1.64
4	0.055~0.0948	11	1.64~2.48
5	0.0948~0.155	12	2.48~3.67
6	0.155~0.257	13	3.67~5.39
7	0.257~0.384	14	5.39~9.92

3.1.3. Microscopic Morphology and Elemental Composition of Particulate Matter

SEM, EDS, and XRD were conducted on particulate matter samples collected before and after the heat exchanger to examine their microstructures, element types, and component analysis. The results are presented in Figure 6. As shown in Figure 6a, before the heat exchanger, the flue gas temperature was high, and SO_3 existed in a gaseous form as H_2SO_4. There were no collisions and adhesions of sulfuric acid droplets with particulate matter. Therefore, the particulate matter was smooth spherical particulate matter at this stage. Figure 6b displays the situation after the heat exchanger, where the flue gas temperature dropped below the dew point. At this point, gaseous H_2SO_4 condensed into sulfuric acid droplets, which collided and adhered to the particulate matter. This led to rougher particulate matter surfaces and partial agglomeration of multiple types of fine particulate matter. From the EDS analysis of the fine particulate matter samples after the heat exchanger, as shown in Figure 6c, it was evident that the sulfur (S) element content in the particulate matter increased significantly, while the content of other elements changed only slightly. This indicated the condensation and adsorption of SO_3 on the particulate matter. In addition, as revealed by the XRD analysis of the particulate matter in Figure 6d, the fly ash particulate matter before the heat exchanger primarily consisted of various metal or non-metal oxides, including $3Al_2O_3 \cdot 2SiO_2$, SiO_2, Al_2O_3, MgO, and CaO. After passing through the heat exchanger, the particulate matter contained not only the substances above but also $MgSO_4$ and $CaSO_4$. This detection of $MgSO_4$ and $CaSO_4$ suggests that they were formed as gaseous H_2SO_4 condensed on the particulate matter surfaces and reacted with magnesium/calcium-containing substances such as MgO and CaO. This further indicates that the SO_3 in the flue gas, after undergoing cooling, condensed onto the fly ash particulate matter and reacted with its alkaline components, resulting in neutralization reactions.

3.2. The Removal Performance of LLT-ESP for SO₃

3.2.1. Removal Performance of LLT-ESP for SO₃ with or without Ash in Flue Gas

To investigate the removal characteristics of SO_3 in the LLT-ESP, the concentration of SO_3 and the removal efficiency before and after the LLT-ESP were studied with and without fly ash. As shown in Figure 7, when the flue gas contained only SO_3, the SO_3 concentration in the flue gas before the heat exchanger was 80.4 mg/m^3, and after passing through the LLT-ESP, it decreased to 50.1 mg/m^3. This indicated that the removal efficiency of individual sulfuric acid droplets in the ESP was approximately 37.7%. When the flue gas contained both SO_3 and fly ash, the concentration of SO_3 in the flue gas before the heat exchanger was 81.0 mg/m^3. After passing through the LLT-ESP, the concentration of SO_3 decreased to 25.5 mg/m^3, resulting in a removal efficiency of 68.5% for SO_3 in the presence of fly ash. These results indicated that in the absence of fly ash, sulfuric acid droplets formed by homogeneous nucleation had smaller particulate matter sizes and larger quantities, leading to a lower removal efficiency by the ESP. However, when fly ash particulate matter was present in the flue gas, SO_3 could condense on this particulate matter through both homogeneous and heterogeneous nucleation, enhancing the overall removal efficiency of SO_3 by the LLT-ESP. This underscored the significant role of fly ash particulate matter in the removal of SO_3 during the LLT-ESP process.
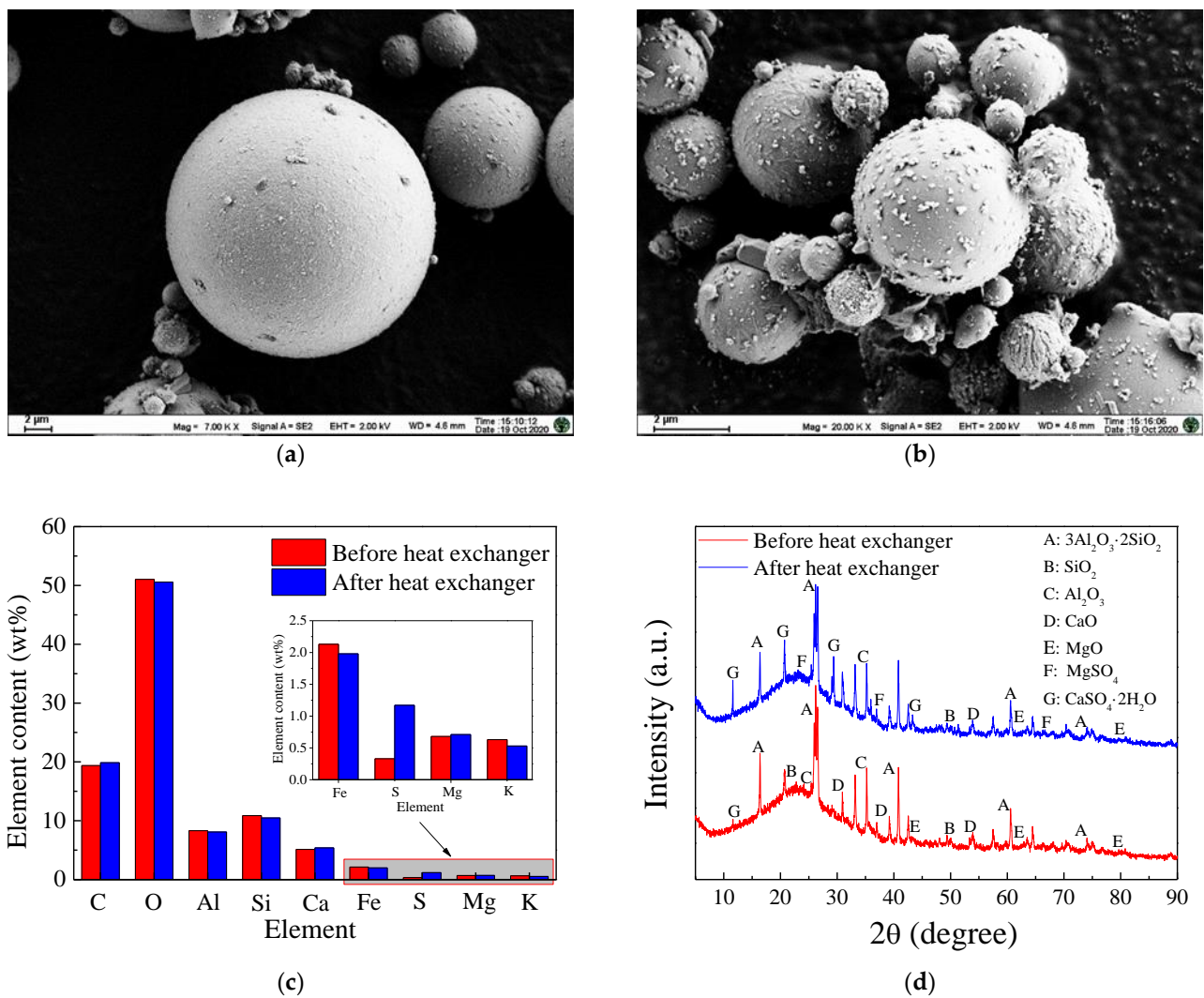
Figure 6. Micro-morphology, elemental, and component analysis of ash before and after heat exchanger. (**a**) SEM before heat exchanger, (**b**) SEM after heat exchanger, (**c**) EDS, (**d**) XRD.

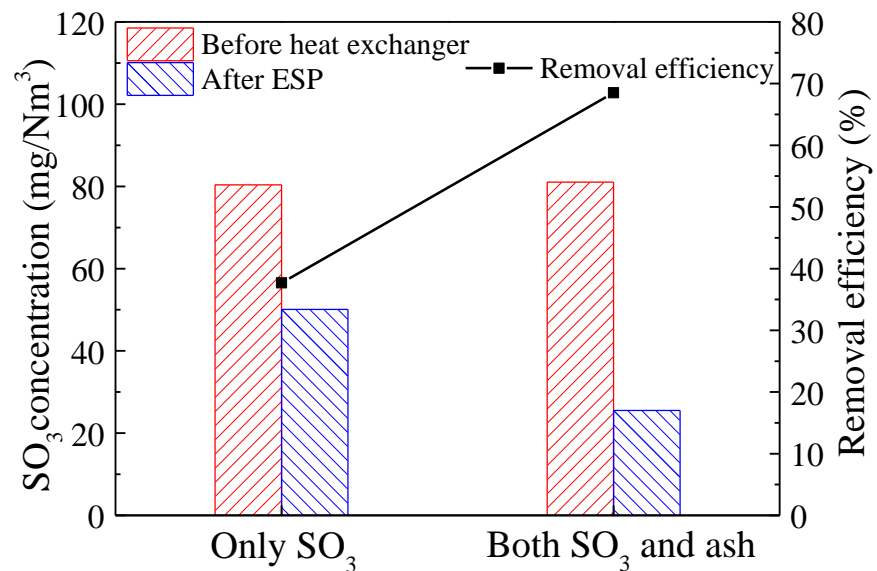**Figure 7.** SO_3 concentration in flue gas and removal efficiency before and after LLT-ESP with and without ash (ash concentrations of 12g/Nm^3, flue gas temperatures of 70 °C).

3.2.2. Influence of Ash Concentration on SO_3 Removal Performance

Due to the significant impact of the SO_3 condensation in fly ash on the removal efficiency during the LLT-ESP process, we investigated the influence of fly ash concentration on SO_3 removal efficiency by adjusting the ash injection rate from the aerosol generator. As shown in Figure 8, with an increase in the ash injection rate, the concentration of fly ash in the flue gas increased from 4 g/m^3 to 20 g/m^3. Consequently, the SO_3 concentration after the LLT-ESP decreased from 47.6 mg/m^3 to 20.4 mg/m^3, and the removal efficiency of SO_3 increased from 40.6% to 74.8%. These results demonstrated that an elevated concentration of fly ash in the flue gas improved the removal efficiency of SO_3. This was primarily due to the increase in particulate matter quantity as fly ash concentration increased. According to the previous study on the condensation characteristics of SO_3, a higher particulate matter concentration was favorable for enhancing SO_3 condensation on the particulate matter, allowing it to be captured and removed by the ESP. Furthermore, when the fly ash concentration in the flue gas was below 12 g/m^3, the increase in SO_3 removal efficiency was more significant with higher fly ash concentration. However, when the fly ash concentration exceeded 12 g/m^3, the increase in SO_3 removal efficiency became less pronounced. This indicated that when the particulate matter concentration in the flue gas reached a relatively high level, some of the condensed sulfuric acid droplets were still unable to effectively collide and adhere to the particulate matter, resulting in incomplete removal by the LLT-ESP.
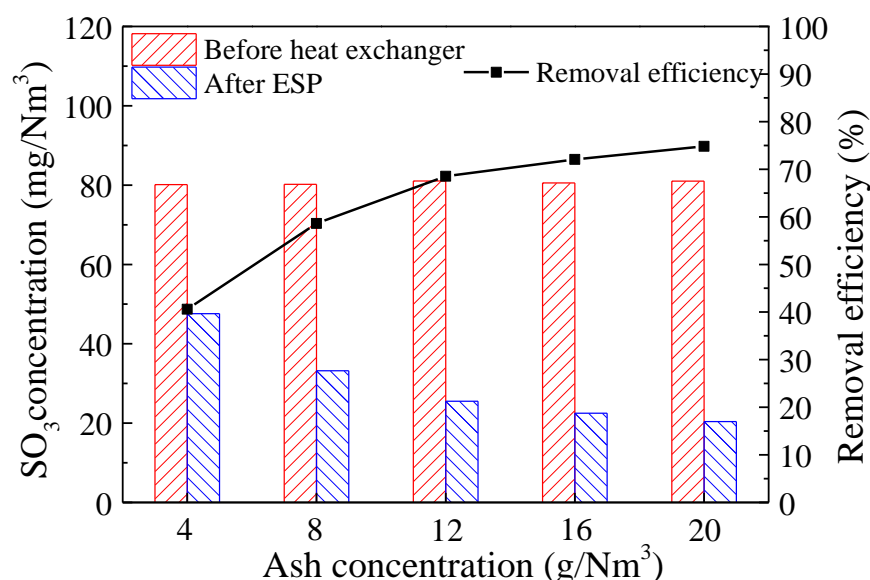

Figure 8. SO_3 concentration in flue gas and removal efficiency before and after LLT-ESP at different ash concentrations (both SO_3 and ash presented, flue gas temperatures of 70 °C).

3.2.3. Influence of Flue Gas Temperature on SO_3 Removal Effect

In the LLT-ESP process, the post-heat exchanger flue gas temperature significantly impacted the condensation of SO_3, thereby influencing the effectiveness of SO_3 removal. Therefore, by adjusting the flow rate of cooling water within the heat exchanger to control the post-heat exchanger flue gas temperature, we investigated the effects of different flue gas temperatures on SO_3 removal. Figure 9 depicts the concentration and removal efficiency of SO_3 before and after the LLT-ESP at various flue gas temperatures. The results indicated that when the post-heat exchanger flue gas temperature was between 70 and 110 °C, the concentration of SO_3 after ESP remained nearly constant, and its removal efficiency was consistently around 68.6%. Subsequently, as the post-heat exchanger flue gas temperature increased further, the removal efficiency of SO_3 in the LLT-ESP rapidly declined. At 130 °C, the removal efficiency dropped to 24.2%, and at 150 °C, it further decreased to 17.7%. It could be inferred that in this experiment, the acid dew point of SO_3 was between 110 °C and 130 °C. When the post-heat exchanger flue gas temperature

was below the acid dew point, SO_3 in the flue gas effectively condensed and coalesced on fine ash particulate matter, subsequently being removed by the ESP along with the fine particles. However, when the post-heat exchanger flue gas temperature exceeded the acid dew point, SO_3 in the flue gas could not effectively condense. Since the ESP was primarily designed for solid pollutant removal, its efficiency in removing gaseous pollutants was poor, leading to a sharp decrease in the removal efficiency of SO_3. This highlighted the critical importance of controlling the post-heat exchanger flue gas temperature in the low-temperature electrostatic precipitation process for the removal of SO_3 from the flue gas. Simultaneously, it emphasized the significant impact of the condensation of SO_3 on fly ash in the flue gas on its removal efficiency.
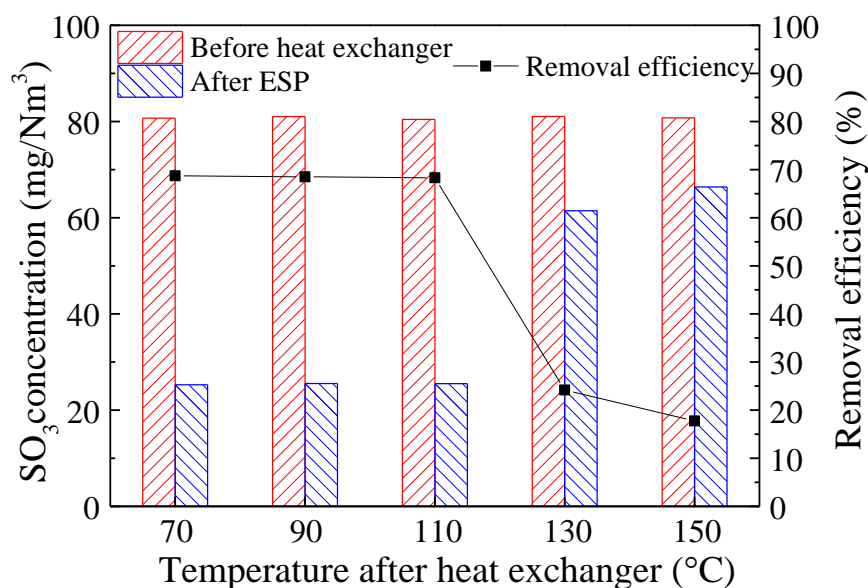

Figure 9. SO_3 concentration and removal efficiency before and after LLT-ESP at different flue gas temperatures (both SO_3 and ash presented, ash concentrations of 12 g/Nm^3).

4. Conclusions

In this work, to facilitate the synergistic removal of SO_3 and fine particulate matter in coal-fired flue gas by an LLT-ESP, a simulated experimental system was designed and constructed to systematically investigate the condensation and removal characteristics of SO_3 during the LLT-ESP process. The main conclusions are as follows:

During the LLT-ESP process, gaseous H_2SO_4 simultaneously underwent heterogeneous and homogeneous condensation. Sulfuric acid droplets formed by the condensation of SO_3 tended to condense on smaller particulate matter, evidenced by the EDS analysis results and the formation of the MgSO4 component. After passing through the heat exchanger, the increase in SO_3 mass concentration in fine particulate matter below 1.0 μm was most significant, rising from 45.6 μg/mg to 152.7 μg/mg.

In the process of LLT-ESP removal of SO_3, the presence of fly ash fine particulate matter was crucial for its removal effectiveness. As the fly ash concentration in the flue gas increased from 4 g/m^3 to 20 g/m^3, the removal efficiency of SO_3 gradually increased. However, when the fly ash concentration exceeded 12 g/m^3, the increase in SO_3 removal efficiency became slower, indicating that even at this point, some condensed sulfuric acid droplets could not effectively collide and adhere to fine particulate matter, preventing its synergistic removal by ESP.

In the LLT-ESP process, the removal efficiency of SO_3 rapidly increased as the flue gas temperature dropped after the heat exchanger. When the flue gas temperature after the heat exchanger was below the acid dew point, SO_3 in the flue gas could effectively condense and coalesce on fine ash particulate matter. This phenomenon occurred concurrently with the ESP's coordinated removal of fine particulate matter.

References

1. Badran, M.; Mansour, A.M. Evaluating performance indices of electrostatic precipitators. *Energies* **2022**, *15*, 6647. [CrossRef]
2. Bin, H.; Yang, Y.; Shu, P.; Liang, C.; Roszak, S.; Yang, L. SO_3 reduction in the flue gas by adding a chemical agent. *Energy Fuels* **2017**, *31*, 12399–12406. [CrossRef]
3. Qi, Z.; Li, J.; Wu, D.; Xie, W.; Li, X.; Liu, C. Particulate matter emission characteristics and removal efficiencies of a low-low temperature electrostatic precipitator. *Energy Fuels* **2017**, *31*, 1741–1746. [CrossRef]
4. Zheng, C.; Wang, L.; Zhang, Y.; Zhang, J.; Zhao, H.; Zhou, J.; Gao, X.; Cen, K. Partitioning of hazardous trace elements among air pollution control devices in ultra-low-emission coal-fired power plants. *Energy Fuels* **2017**, *31*, 6334–6344. [CrossRef]
5. Gao, H.; Long, Z.; Feng, Z.; Lin, B.; Yu, T. Numerical simulation of the characteristics of oil mist particles deposition in electrostatic precipitator. *Process Saf. Environ. Prot.* **2022**, *164*, 335–344. [CrossRef]
6. Gao, M.; Zhu, Y.; Yao, X.; Shi, J.; Shang, G. Dust removal performance of two-stage electrostatic precipitators and its influencing factors. *Powder Technol.* **2019**, *348*, 13–23. [CrossRef]
7. Gao, W.; Zhang, H.; Wu, Z.; Wang, Y.; Shao, L.; Zheng, C.; Yu, A.; Gao, X. Low-temperature electrostatic precipitator with different electrode configurations under various operation conditions. *Powder Technol.* **2021**, *394*, 1178–1185. [CrossRef]
8. Guo, B.; Yang, D.; Su, Y.; Yu, A. Process modelling of low temperature electrostatic precipitators. *Powder Technol.* **2017**, *314*, 567–576. [CrossRef]
9. Zhou, X.; Tang, W.; He, M.; Xiao, X.; Wang, T.; Cheng, S.; Zhang, L. Combined removal of SO_3 and HCl by modified $Ca(OH)_2$ from coal-fired flue gas. *Sci. Total Environ.* **2023**, *857*, 159466. [CrossRef] [PubMed]
10. Pei, T.; Ma, S.; Zhao, G.; Wang, P.; Song, G.; Mi, C.; Wang, F. Study on the removal characteristics of SO_3 acid mist during the condensation of wet flue gas. *Ind. Eng. Chem. Res.* **2022**, *61*, 3729–3741. [CrossRef]
11. Xu, G.; Chen, F.; Qian, Y.; Lu, P.; Hong, M.; Zhang, Q.; Zhou, Q. Experimental investigation of removal of SO_3 from flue gas with modified fly ash adsorbents. *ACS Omega* **2023**, *8*, 16656–16672. [CrossRef] [PubMed]
12. He, K.; Song, Q.; Yan, Z.; Yao, Q. SO_3 removal from flue gas by using Na_2SO_3. *Energy Fuels* **2020**, *34*, 7232–7241. [CrossRef]
13. Wu, X.; Liu, W.; Gao, H.; Alfaro, D.; Sun, S.; Lei, R.; Jia, T.; Zheng, M. Coordinated effects of air pollution control devices on PAH emissions in coal-fired power plants and industrial boilers. *Sci. Total Environ.* **2021**, *756*, 144063. [CrossRef] [PubMed]
14. Huang, R.; Yu, R.; Wu, H.; Pan, D.; Zhang, Y.; Yang, L. Investigation on the removal of SO_3 in ammonia-based WFGD system. *Chem. Eng. J.* **2016**, *289*, 537–543. [CrossRef]
15. Li, J.; Li, X.; Zhou, C.; Li, M.; Lu, S.; Yan, J.; Qi, Z.; Shou, C. Correlation between polycyclic aromatic hydrocarbon concentration and particulate matter during the removal process of a low-low temperature electrostatic precipitator. *Energy Fuels* **2017**, *31*, 7256–7262. [CrossRef]
16. Yuan, D.; Trabelsi, T.; Zhang, Y.; Francisco, J.; Wang, L. Probing the electronic structure and bond dissociation of SO_3 and SO_3-using high-resolution cryogenic photoelectron imaging. *J. Am. Chem. Soc.* **2022**, *144*, 13740–13747. [CrossRef] [PubMed]
17. Zheng, C.; Li, X.; Yang, Z.; Zhang, Y.; Wu, W.; Wu, X.; Wu, X.; Gao, X. Development and experimental evaluation of a continuous monitor for SO_3 measurement. *Energy Fuels* **2017**, *31*, 9684–9692. [CrossRef]
18. Li, X.; Li, J.; Wu, D.; Lu, S.; Zhou, C.; Qi, Z.; Li, M.; Yan, J. Removal effect of the low-low temperature electrostatic precipitator on polycyclic aromatic hydrocarbons. *Chemosphere* **2018**, *211*, 44–49. [CrossRef]
19. Sun, K.; Yan, Y.; Jiang, J.; Deng, L.; Che, D. SO_3 removal efficiency and ash particle flowability of low-low-temperature flue gas systems (LLTSs). *Appl. Therm. Eng.* **2020**, *171*, 115132. [CrossRef]
20. Li, X.; Zhou, C.; Li, J.; Lu, S.; Yan, J. Distribution and emission characteristics of filterable and condensable particulate matter before and after a low-low temperature electrostatic precipitator. *Environ. Sci. Pollut. Res.* **2019**, *26*, 12798–12806. [CrossRef]
21. Liu, F.; Yu, D.; Han, J.; Wu, J.; Yu, X.; Gong, X. Effects of ultra-low emission air pollution control devices on the evolution of PM and its associated water-soluble ions in a 1000 MW coal-fired power plant. *Fuel* **2023**, *343*, 127931. [CrossRef]

22. Lv, G.; Sun, X. The role of air-water interface in the SO$_3$ hydration reaction. *Atmos. Environ.* **2020**, *230*, 117514. [CrossRef]
23. Zheng, C.; Hong, Y.; Xu, Z.; Li, C.; Wang, L.; Yang, Z.; Zhang, Y.; Gao, X. Experimental study on removal characteristics of SO$_3$ by wet flue gas desulfurization absorber. *Energy Fuels* **2018**, *32*, 6031–6038. [CrossRef]
24. Pan, D.; Zhang, D.; Zhang, W. Investigation on removal characteristics of SO$_3$ acid mist during limestone-gypsum desulfurization process. *Energy Fuels* **2018**, *32*, 12949–12954. [CrossRef]
25. Wang, R.; Cheng, Y.; Hu, Y.; Chen, S.; Guo, X.; Song, F.; Li, H.; Zhang, T. Reaction of SO$_3$ with H$_2$SO$_4$ and its implication for aerosol particle formation in the gas phase and at the air-water interface. *EGUsphere* **2023**, *2023*, 1–31.
26. Zheng, C.; Wang, Y.; Liu, Y.; Yang, Z.; Qu, R.; Ye, D.; Liang, C.; Liu, S.; Gao, X. Formation, transformation, measurement, and control of SO$_3$ in coal-fired power plants. *Fuel* **2019**, *241*, 327–346. [CrossRef]
27. Zheng, C.-H.; Wang, L.; Zhang, Y.-X.; Weng, W.-G.; Zhao, H.-T.; Zhou, J.-S.; Gao, X. Co-benefit of hazardous trace elements capture in dust removal devices of ultra-low emission coal-fired power plants. *J. Zhejiang Univ. Sci. A* **2018**, *19*, 68–79. [CrossRef]
28. Wu, Y.; Xu, Z.; Huang, X.; Liu, S.; Tang, M.; Lu, S. A typical 300 MW ultralow emission coal-fired power plant: Source, distribution, emission, and control of polycyclic aromatic hydrocarbons. *Fuel* **2022**, *326*, 125052. [CrossRef]
29. Romero, C.; Vahedi, N.; Yao, Z.; Stenger, H. Modeling of SO$_3$ formation and depletion processes in coal-fired boilers. *Fuel* **2020**, *280*, 118355. [CrossRef]
30. Zheng, C.; Luo, C.; Liu, Y.; Wang, Y.; Lu, Y.; Qu, R.; Zhang, Y.; Gao, X. Experimental study on the removal of SO$_3$ from coal-fired flue gas by alkaline sorbent. *Fuel* **2020**, *259*, 116306. [CrossRef]
31. *HJ 544-2016*; Stationary Source Emission-Determination of Sulfuric Acid Mist-Ion Chromatography. Ministry of Ecology and Environment of the People's Republic of China: Beijing, China, 2016. Available online: https://www.mee.gov.cn/ywgz/fgbz/bz/bzwb/jcffbz/201604/t20160405_334680.shtml (accessed on 29 March 2016).
32. Yang, Z.; Zheng, C.; Zhang, X.; Zhou, H.; Silva, A.A.; Liu, C.; Snyder, B.; Wang, Y.; Gao, X. Challenge of SO$_3$ removal by wet electrostatic precipitator under simulated flue gas with high SO$_3$ concentration. *Fuel* **2018**, *217*, 597–604. [CrossRef]
33. Larson, L.J.; Kuno, M.; Tao, F.-M. Hydrolysis of sulfur trioxide to form sulfuric acid in small water clusters. *J. Chem. Phys.* **2000**, *112*, 8830–8838. [CrossRef]
34. Mertens, J.; Bruns, R.; Schallert, B.; Faniel, N.; Khakharia, P.; Albrecht, W.; Goetheer, E.; Blondeau, J.; Schaber, K. Effect of a gas-gas-heater on H$_2$SO$_4$ aerosol formation: Implications for mist formation in amine based carbon capture. *Int. J. Greenh. Gas Control* **2015**, *39*, 470–477. [CrossRef]
35. Yang, L.; Bao, J.; Yan, J.; Liu, J.; Song, S.; Fan, F. Removal of fine particles in wet flue gas desulfurization system by heterogeneous condensation. *Chem. Eng. J.* **2010**, *156*, 25–32. [CrossRef]